

Article

Design, Kinematics and Controlling a Novel Soft Robot Arm with Parallel Motion

Alaa Al-Ibadi ^{1,2,*} , Samia Nefti-Meziani ¹ and Steve Davis ¹

¹ School of Computing, Science & Engineering, University of Salford, Salford M5 4WT, UK; S.Nefti-Meziani@salford.ac.uk (S.N.-M.); S.T.Davis@salford.ac.uk (S.D.)

² Computer Engineering Department, University of Basrah, Basrah 61004, Iraq

* Correspondence: a.f.a.al-ibadi@edu.salford.ac.uk or alaa.falah77@ieee.org; Tel.: +44-743-846-2585

Received: 19 March 2018; Accepted: 16 May 2018; Published: 17 May 2018



Abstract: This article presents a novel design for a double bend pneumatic muscle actuator (DB-PMA) inspired by snake lateral undulation. The presented actuator has the ability to bend in opposite directions from its two halves. This behavior results in horizontal and vertical movements of the actuator distal ends. The kinematics for the proposed actuator are illustrated and experiments conducted to validate its unique features. Furthermore, a continuum robot arm with the ability to move in parallel (horizontal displacement) is designed with a single DB-PMA and a two-finger soft gripper. The performance of the soft robot arm presented is explained, then another design of the horizontal motion continuum robot arm is proposed, using two self-bending contraction actuators (SBCA) in series to overcome the payload effects on the upper half of the soft arm.

Keywords: snake lateral undulation locomotion; double bend pneumatic muscle actuator (DB-PMA); self-bending contraction actuator (SBCA); soft robot arm; horizontal motion

1. Introduction

Biological concepts provide significant inspirations for human creation. The robot is one of these inspirations; researchers around the world have converted the fundamentals of biological movements to mechanical forms. Robots resembling humans, dogs, geckos, snakes, and other types of animal, have been designed [1–6]. Several types of actuators used in robotics are also inspired by biology.

Since the early 2000s, an alternative form of the rigid robot has been developed by using a soft muscle-like actuator called the pneumatic muscle actuator (PMA). This development has led to the development of soft robotics, which is considered to be a new generation of robotics. The PMA, which was developed by McKibben in the 1950's, is constructed from an inner rubber tube covered by a braided sleeve and closed from both sides with a small inlet [7]. The PMA has been modelled by numerous researchers. Among these models is the tensile force model [7] and the contractile force model introduced by [8]. Enhancements of these models were presented by [9–13].

The length of the PMA was modelled geometrically by Doumit, M., et al. [14]; the formula length depends on the length of the braided strand, diameter, braided angle, and number of strand turns. Al-Ibadi, A. et al. [12] formulated the length of the contraction actuators as a sigmoidal function depending on the applied pressure and initial length.

The PMA is designed to either contract or extend according to the braided angle and the implementation method. The braided angle θ less than 54.7° contracts the actuator by a contraction ratio ϵ to about 30%. The extension behavior occurs when θ is greater than 54.7° at an extension ratio $\acute{\epsilon}$ of about 50% [12,15,16].

The basic behavior of the PMA involves linearly contracting or extending; however, developments have been proposed to improve the behavior by modifying its structure. A bending performance was presented

by numerous researchers, including the PneuNet actuator by Ilievski, F., et al. [17]. The authors presented a bending actuator by changing the wall's thickness. This actuator is easy to manufacture, but the ratio of the elasticity that was achieved was too limited. To overcome this limitation, Deimel, R., et al. [18] used a PneuFlex actuator that implants polymer fibers to reinforce the rubber substrate. The elasticity of the polyethylene terephthalate (PET) material was three to four times less than silicon. Al-Ibadi, A., et al. [19] designed a self-bending contraction actuator (SBCA) by inserting a reinforced flexible rod to one side of the contraction PMA to achieve bending behavior. Al-Fahaam, H., et al. [20] proposed enabling bending behavior by modifying the structure of the extensor PMA by using a high-tension thread to reinforce one side of the covered sleeve. Faudzi, A.A.M., et al. [21] used the effect of the braided angle on the actuator performance to design a bending behavior by using two different braided sleeves of different braided angles to cover the inner tube of the contractor PMA.

Snake propulsion patterns are used to design snake robots to achieve several goals, such as rescue missions after natural and man-made disasters, inspections, investigations, and maintenance for dangerous or narrow areas [22–24]. The multiple links snake robot was designed by Shan, Y., et al. [25] by using direct current (DC) motors to control the angles between the links and solenoids with sharp tip pins to generate a push force to the ground, and provide forward movement by moving the joints in a lateral direction. A wheel snake-like robot, SAM, was presented by Yamakita, M., et al. [26]. The friction between the wheels and the ground was ignored. A series of multi-module snake robots were designed by Wright, C., et al. [27], and the joint angle was controlled by a servo motor via a proportional–integral–derivative (PID) control system. Wright, C., et al. [28] designed a serial-linkage snake robot that contained several rigid modules with a DC motor and a gear box for each, resulting in an extendable 16 degrees of freedom (DOF).

The main contribution in this article is the design of a DB-PMA inspired by the shape of snake lateral undulation locomotion. We present the kinematics for the proposed actuator; then, a soft arm is designed using the new actuator. A modified version of the continuum arm is presented by using the SBCA.

In this article, the motion principle of the snake is explained in Section 2, which is then used to propose a double bend pneumatic muscle actuator (DB-PMA) in Section 3. The kinematics of the proposed actuator are presented and validated experimentally in Sections 4 and 5, respectively. A two-finger soft gripper based on SBCA is designed, implemented, and attached to the end of the DB-PMA to design a soft robot arm for horizontal displacement. Then, another design of the horizontal motion continuum arm is presented by using two SBCA in series. The performance of both the proposed continuum robot arms are illustrated and validated by a control system in Section 6.

2. Snake Motion

Snake propulsion can be classified into four patterns: lateral undulation (serpentine), rectilinear locomotion, sidewinding, and concertina progression [23,24,29]. Lateral undulation is the most effective locomotion mode and it is widely perceived in almost all kinds of snakes. For this reason, we chose this pattern for our research. The snake forms its body into several curves, positioning in the X-Y planes during the lateral undulation. Figure 1 shows the lateral undulation locomotion of a snake.



Figure 1. The lateral undulation locomotion of a snake.

3. Structure of the Double-Bend Actuator

The basic structure of the contraction PMA is shown in Figure 2. The length of the braided sleeve was assumed to be similar to the length of the inner rubber tube to ensure that the braided angle θ is less than 54.7° . Figure 1 shows how the snake bends its body several times in two directions. The shape and the performance of this bending pattern were used to design a double bend pneumatic muscle actuator (DB-PMA) by inserting two thin reinforcement rods between the rubber tube and the sleeve. Each rod was placed on opposite sides of the two halves of the contraction actuator as illustrated in Figure 3. Each rod was three-dimensional (3D) printed with length of 28 cm, width of 0.6 cm, and height of 0.1 cm.

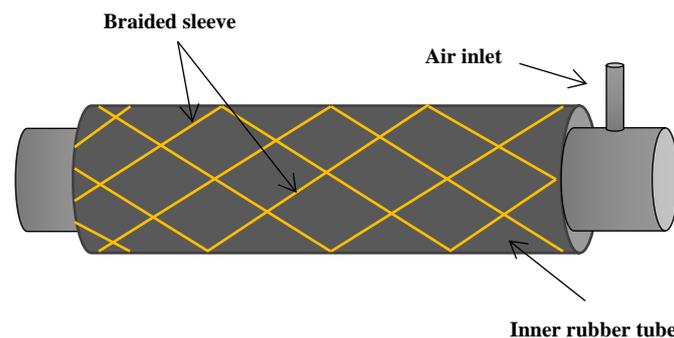


Figure 2. The structure of the contraction pneumatic muscle actuator (PMA).

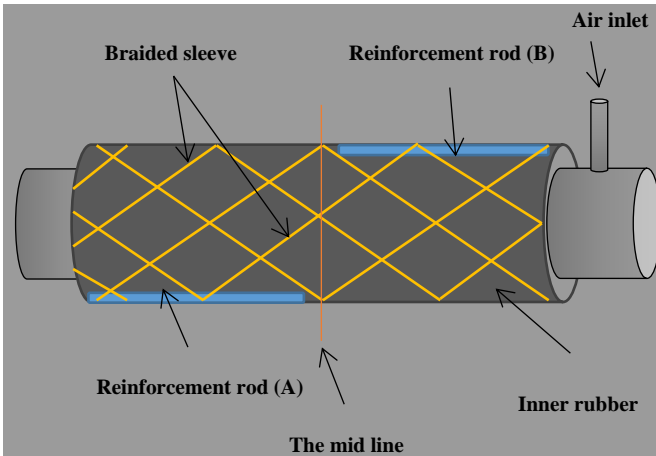


Figure 3. The structure of the double bend pneumatic muscle actuator (DB-PMA).

The contraction occurs on the free sides while the rods prevent it, which leads to a bending behavior as shown in Figure 4.

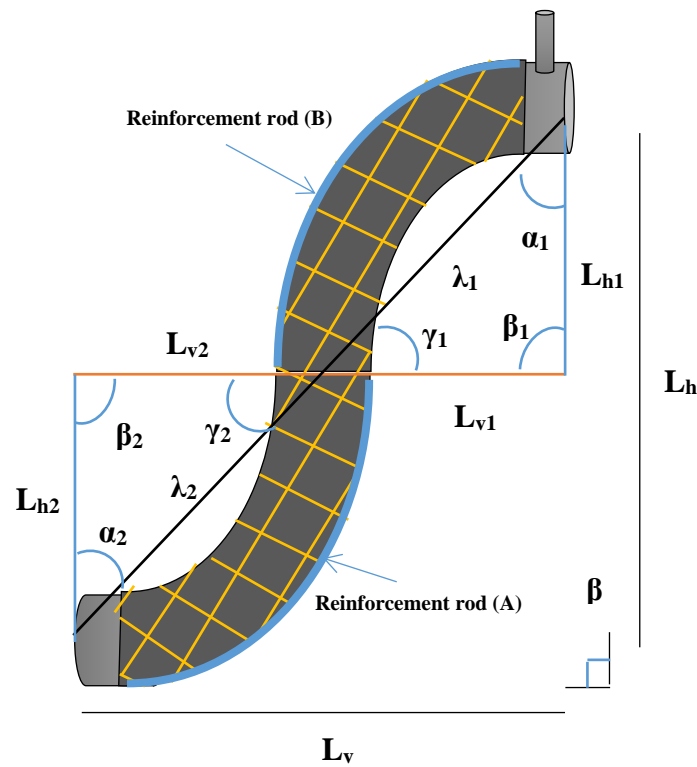


Figure 4. The bending behavior and the geometrical analysis of the DB-PMA.

4. Kinematics of the DB-PMA

The geometrical analysis of the proposed arm is illustrated in Figures 3 and 4 in two conditions according to the applied pressure: a relaxed and a pressurized condition.

4.1. Relaxed Condition

The length of the DB-PMA at zero pressure can be described with Equation (1):

$$L_v = \lambda = L_0 \tag{1}$$

where:

$$\lambda = \lambda_1 + \lambda_2 \tag{2}$$

where L_v is the vertical actuator length and L_0 is the actuator length at zero pressure.

Hence, the length of the double-bend actuator is divided into two components: the vertical length and the horizontal length. Due to the relaxed condition, the horizontal length of the DB-PMA is zero.

4.2. Pressurised Condition

Figure 4 shows both the vertical and horizontal lengths of the DB-PMA under pressurised conditions. The proposed actuator moves horizontally by the summation of the horizontal components of the first and the second halves, as shown in Equation (3).

$$L_h = L_{h1} + L_{h2} \tag{3}$$

where L_h is the total horizontal movement with respect to the section area of the actuator, L_{h1} is the horizontal length of the first half, and L_{h2} is the horizontal length of the second half.

Both the vertical and horizontal movements can be calculated by using the cosine law as shown in Equation (4):

$$\lambda_1^2 = L_{v1}^2 + L_{h1}^2 - 2L_{v1}L_{h1}\cos\beta_1 \quad (4)$$

where λ_1 is the distance between the first end and the mid line of the actuator and β_1 is the angle between the direction of the vertical and horizontal distances of the first half.

Similarly, the distance between the second end and the mid line (λ_2) of the actuator under a pressurised condition is described in Equation (5):

$$\lambda_2^2 = L_{v2}^2 + L_{h2}^2 - 2L_{v2}L_{h2}\cos\beta_2 \quad (5)$$

From Figure 4, both the vertical and the horizontal lengths of the proposed actuator can be found as follows:

$$L_v = (\lambda_1^2 + L_{h1}^2 - 2\lambda_1L_{h1}\cos\alpha_1)^{\frac{1}{2}} + (\lambda_2^2 + L_{h2}^2 - 2\lambda_2L_{h2}\cos\alpha_2)^{\frac{1}{2}} \quad (6)$$

and:

$$L_h = (\lambda_1^2 + L_{v1}^2 - 2\lambda_1L_{v1}\cos\gamma_1)^{\frac{1}{2}} + (\lambda_2^2 + L_{v2}^2 - 2\lambda_2L_{v2}\cos\gamma_2)^{\frac{1}{2}} \quad (7)$$

Alternatively, the angles can be calculated in terms of the distances as follows:

$$\beta_i = \cos^{-1} \frac{L_{vi}^2 + L_{hi}^2 - \lambda_i^2}{2L_{vi}L_{hi}}, (i \in R) \quad (8)$$

where i is either 1 or 2 according to which half of the angle is being calculated.

$$\alpha_i = \cos^{-1} \frac{\lambda_i^2 + L_{hi}^2 - L_{vi}^2}{2\lambda_iL_{hi}}, (i \in R) \quad (9)$$

and:

$$\gamma_i = \cos^{-1} \frac{\lambda_i^2 + L_{vi}^2 - L_{hi}^2}{2\lambda_iL_{vi}}, (i \in R) \quad (10)$$

4.3. Special Condition1

For identical reinforcement rods with similar material and dimensions, the lengths and angles of the presented actuator at pressurised conditions are:

$$L_{v1} = L_{v2} \quad (11)$$

$$L_{h1} = L_{h2} \quad (12)$$

$$\lambda_1 = \lambda_2 \quad (13)$$

$$\beta_1 = \beta_2 = 90^\circ \quad (14)$$

$$\alpha_1 = \alpha_2 \quad (15)$$

$$\gamma_1 = \gamma_2 \quad (16)$$

4.4. Special Condition2

If the bending angles of the first and the second halves equal 90° , then:

$$\alpha_1 = \alpha_2 = \gamma_1 = \gamma_2 = 45^\circ \quad (17)$$

and:

$$L_{v1} = L_{v2} = L_{h1} = L_{h2} \quad (18)$$

or:

$$L_v = L_h = \frac{L_0}{2} \tag{19}$$

or:

$$L_v + L_h = L_0 \tag{20}$$

5. Experiments and Validations

Two identical 28 cm reinforcement rods were placed in the two halves of a 60 cm contraction actuator to create a DB-PMA. Special case 1 was used to calculate the angles and distances for the DB-PMA. Two (HC-SR04) ultrasonic sensors by (ElecFreaks, Shenzhen, China) were used to measure the vertical (L_v) and the horizontal (L_h) distances for the presented actuator. Figure 5 illustrates the presented actuator at two different pressures.

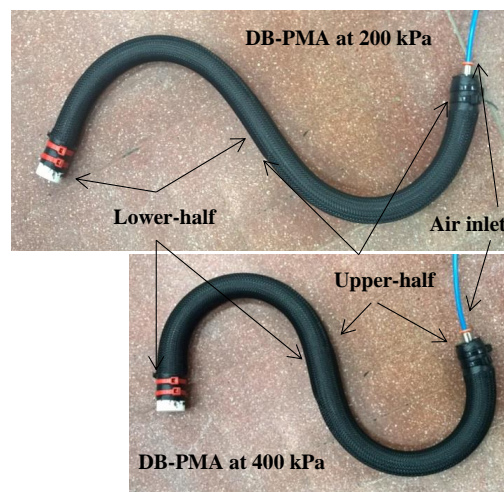


Figure 5. The presented DB-PMA at two different air pressures.

The pressure was applied by using a Matrix 3/3 solenoid valve in 50 kPa steps. At each pressure step, both the vertical and horizontal distances were measured by sensors and the angles were manually measured for several repeats and the average was recorded.

Figure 6a–f show the experiment and validation results for the distances and angles of the presented actuator.

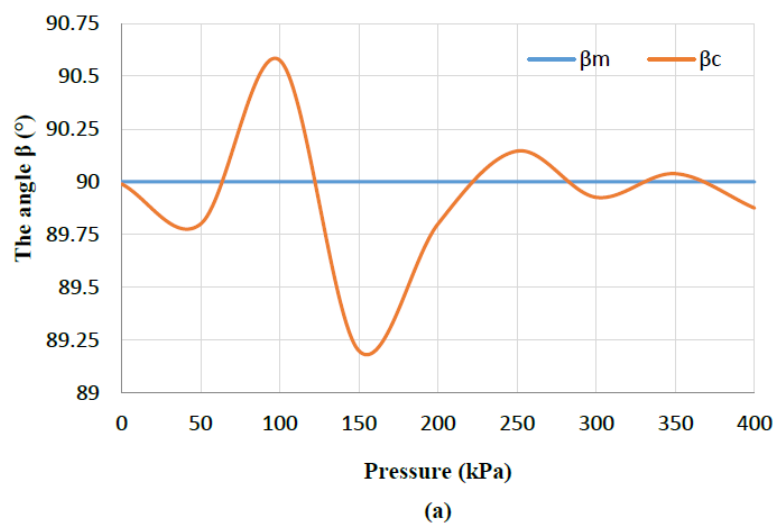


Figure 6. Cont.

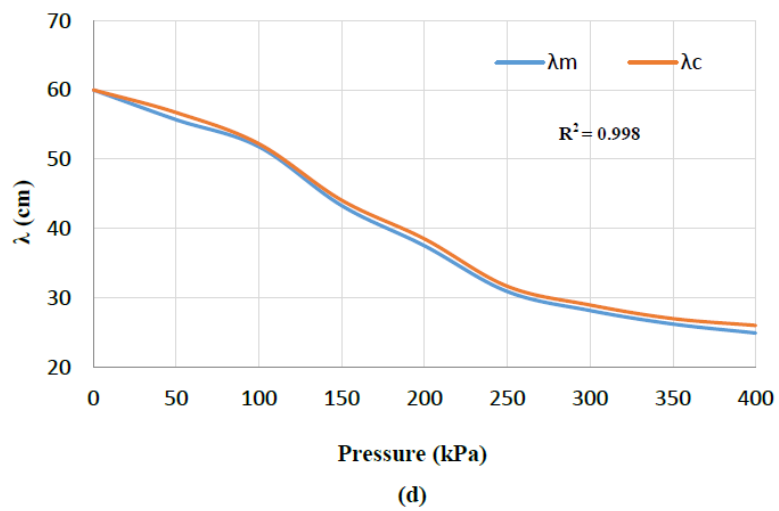
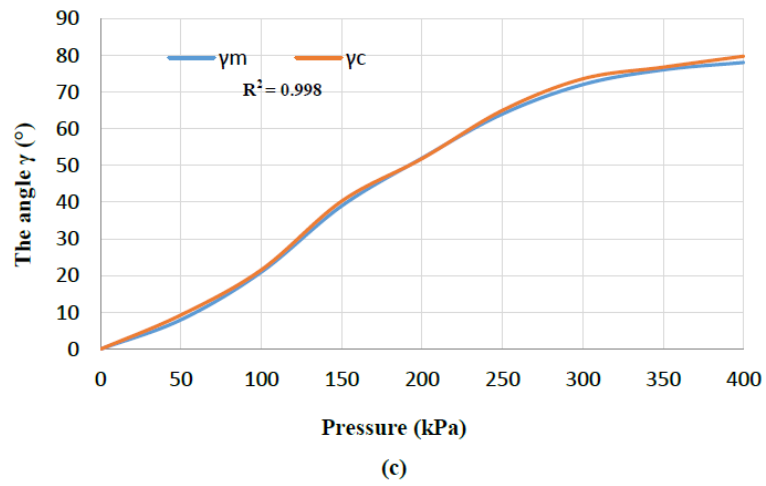
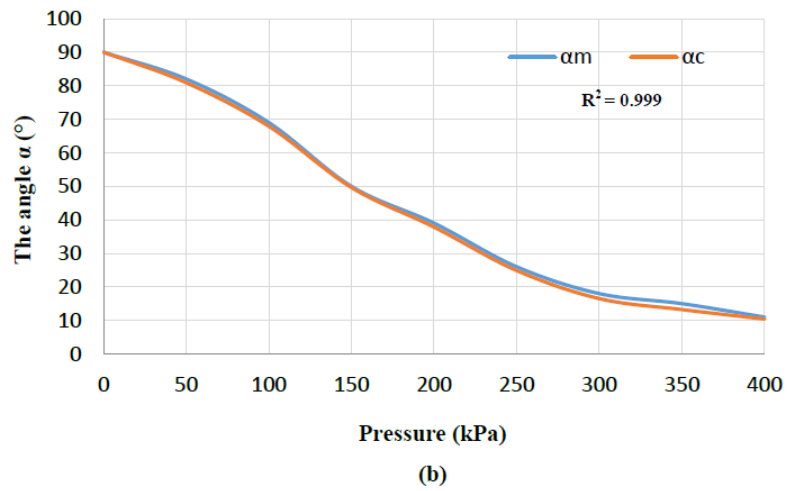
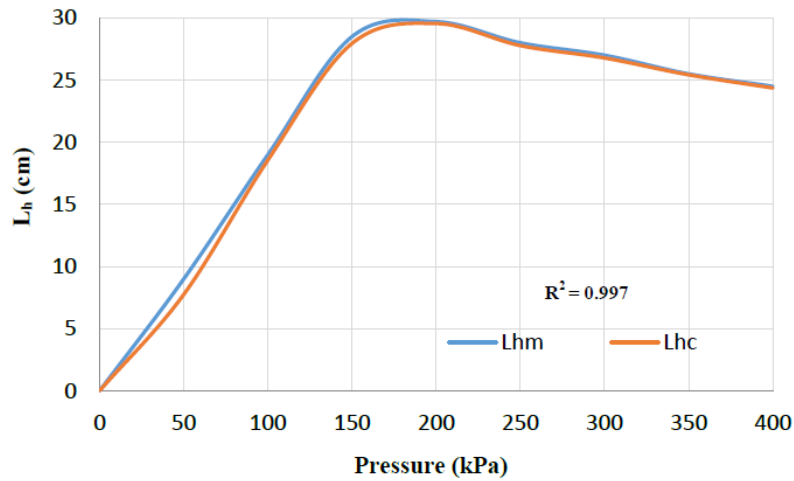
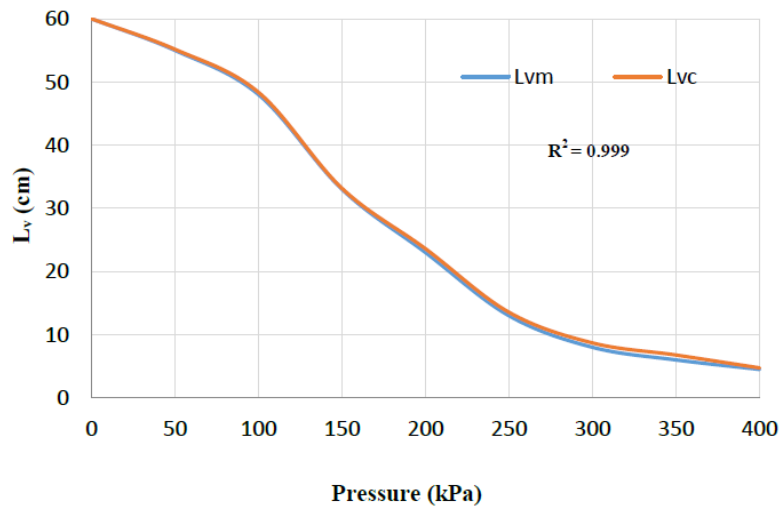


Figure 6. Cont.



(e)



(f)

Figure 6. The parameters of the DB-PMA as a function of air pressure: (a) β_m and the calculated β_c angle, (b) α_m and the calculated α_c angle, (c) γ_m and the calculated γ_c angle, (d) λ_m and the calculated λ_c distance between the two ends, (e) L_{hm} and the calculated L_{hc} horizontal distance, and (f) L_{vm} and the calculated L_{vc} vertical distance.

Figure 6a shows the calculation and the measurement value of β . Since the actuator is designed under special case 1, β has to be 90° . The measured angle is similar to the designed angle, with a maximum error of 0.6° . Because β is constant, α decreases from 90° to 10° (Figure 6b), whereas γ increases from 0° to 80° , as shown in Figure 6c, so that the summation of the triangle angles is 180° at each pressure step.

Figure 6d illustrates the performance of λ with the increase in the applied air pressure. This distance decreases when the pressure increases from the original length of the actuator to about 25 cm at 400 kPa. When the horizontal distance in Figure 6e was changed from 0 to 24.3 cm, through to its maximum value of 30 cm, the maximum change in horizontal direction occurred with special case 2 when both α and γ were about 45° . Figure 6f shows that L_v decreases continuously with pressure increase.

The maximum variation ratio in the horizontal (ε_h) and vertical (ε_v) distances are defined in Equations (21) and (22) as follows:

$$\varepsilon_h = \frac{L_0 - L_h}{L_0} \tag{21}$$

and:

$$\varepsilon v = \frac{L_0 - L_v}{L_0} \quad (22)$$

where L_0 is the initial length of the actuator at relaxed conditions according to the designed dimensions. The maximum ratios for the horizontal and vertical distances are 0.5 and 0.83, respectively. In comparison with the simple contraction PMA, the DB-PMA can be considered an efficient alternative in terms of the contraction ratio between the two ends of the actuator.

6. Horizontal Moving Soft Robot Arm

The proposed DB-PMA can be used as a soft robot arm for moving an object horizontally and vertically by a distance that depends on the pressure and weight of the object. A soft gripper was mounted at the end of the DB-PMA to grasp an object and move it horizontally to another position.

The soft gripper was made by using two 15-cm self-bending contraction actuators (SBCA), as seen in Figure 7. To maximize the range of motion of the fingers, a thin ribbon of elastomeric material was placed on the rear of each finger to cause the fingers to spread when the actuator is unpressurised.

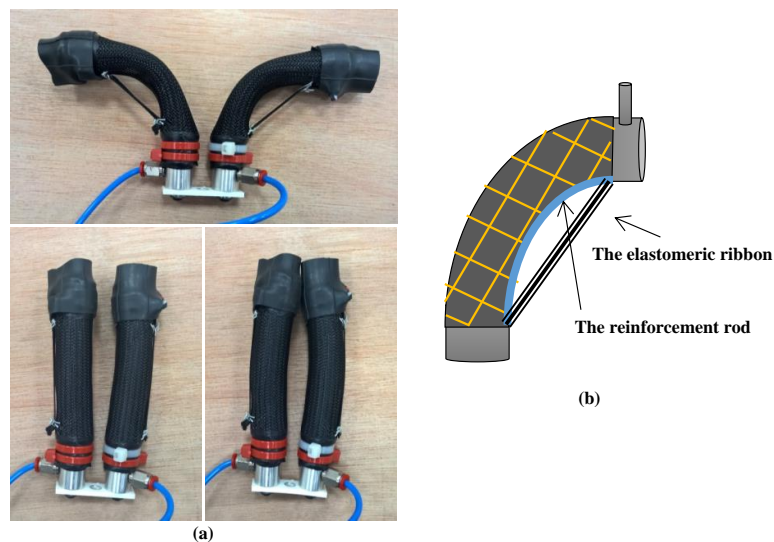


Figure 7. The two-finger soft gripper based on self-bending contraction actuators (SBCA). (a) The soft gripper at different air pressures. (b) The schematic design of the soft finger.

Figure 8 shows the DB-PMA and the two-finger soft gripper as a continuum arm at different pressurized conditions.



Figure 8. The presented continuum robot arm at different pressurized conditions.

To ensure the object will move to the specified position, a neural network (NN) controller was designed to control the horizontal distance of the continuum arm via an ultrasound sensor by controlling the air filling and venting of the actuator via a 3/3 solenoid (Matrix) valve and an Arduino Mega 2560. Figure 9 shows the flowchart of the control system and the DB-PMA. The NARMA-L2 NN-controller included nine neurons in one hidden layer, three-delayed plant inputs, and two-delayed plants outputs, which was trained by (trainlm) for 100 Epochs. The mean square error (MSE) for the training, testing, and validating of the data was about 10^{-7} . The controller output was the pulse width modulation (PWM) signal that controls the air flow for both the filling and venting processes to achieve the desired horizontal position.

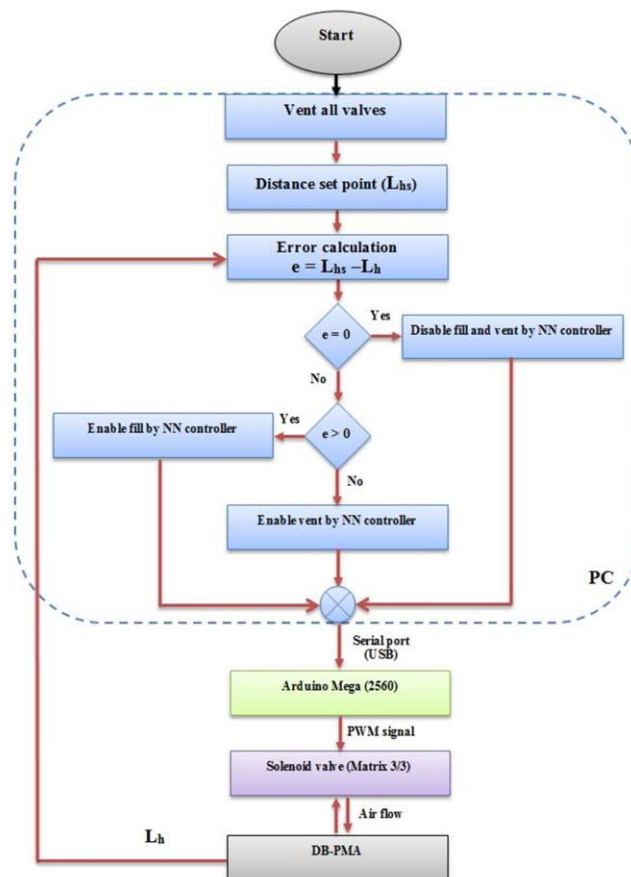


Figure 9. The flowchart of the control system and the DB-PMA.

An approximate model was used to train the neural controller and the actuator length as a function of the duty cycle of the controlled input, which is given by Equation (23):

$$L_h = \frac{0.5L_0 \times u}{98} \tag{23}$$

where L_h is the horizontal distance between the initial position (relaxed condition) and the new position (pressurised condition), u is the controlled duty cycle of the pulse width modulation (PWM) signal, L_0 represents the initial length, the number 98 refers to the 98% of the maximum duty cycle for the control signal to avoid continuous supply to the air valve, and 0.5 is the maximum horizontal distance L_{hmax} (50%) for special case 2.

Step and sinusoidal signals were applied to the controller system at 0.5 Hz, and the response for the horizontal moving process is illustrated in Figure 10a,b.

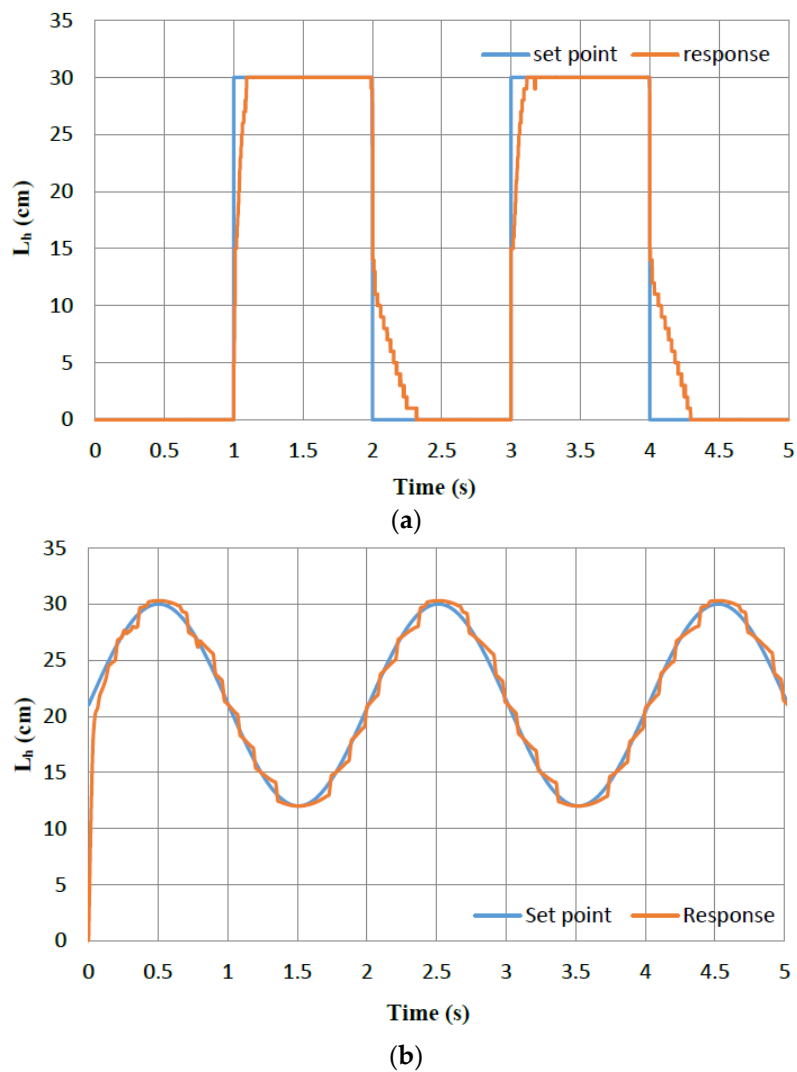


Figure 10. (a) The step response of the horizontal distance at 0.5 Hz. (b) The sinusoidal response of the horizontal distance at 0.5 Hz.

Figure 10a shows that the contraction time was more than the elongation time due to the hysteresis of the actuator material and the pressure difference between the actuator and the outside pressure. The sinusoidal response shows that the L_h is tracking the input signal with low error values.

This process illustrates the ability to use a single soft actuator as an effective robot arm for specific applications at zero or minimum loads. The second half, the gripper and the object, represents a load on the first half (upper-half). This accumulative load reduces the bending angle of the upper-half and places the end of the DB-PMA not in the vertical direction. Two options were possible to overcome the effect of the load condition: either the length of the reinforcement rod increases to increase the bending angle of the upper-half (Table 1) or two identical SBCAs in series are used instead of a single DB-PMA.

Table 1. The maximum bending angle for the three different self-bending contraction actuators (SBCAs) at 500 kPa.

Length of the Actuator and Reinforcement Rod (cm)	Maximum Bending Angle
10	25°
20	125°
30	213°

Figure 11 shows the new horizontal moving continuum arm using the SBCA. This modification ensures the horizontal motion of the continuum robot arm by applying different air pressure.

Using two SBCAs instead of the DB-PMA increased the controlled variables; however, the features were improved. Since each bending actuator is controlled individually, the soft robot arm shows different shapes and performances.

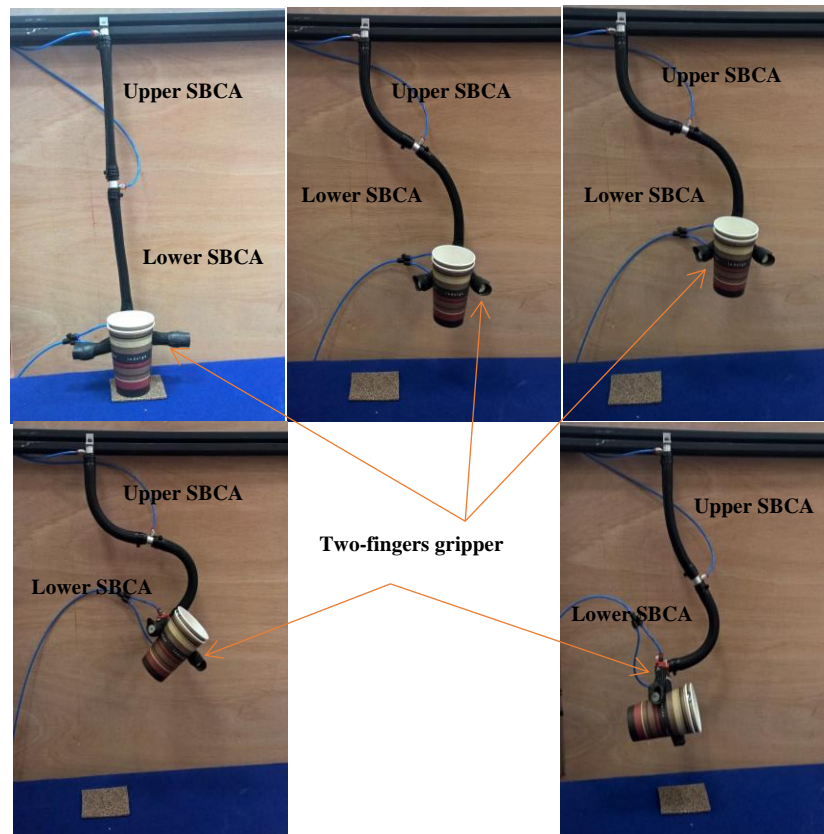


Figure 11. The horizontal moving arm of two SBCAs at different pressurising conditions.

7. Conclusions

We presented a novel double bend pneumatic muscle actuator (DB-PMA) inspired by the lateral undulation of a snake. The kinematics and experiments explained and validated the unique features of the actuator presented. The DB-PMA was used to design a continuum robot arm with the ability of both ends of the actuator to maintain horizontal position so that objects can be moved parallel to the ground. A soft gripper was designed by two SBCAs and attached to the end of the DB-PMA to validate the performance of the soft robot arm. Because the weight of the gripper, the load, and the weight of the lower half affects the resulting bending of the upper half, the presented arm is suitable for working with light loads. To increase the efficiency of the presented arm, two SBCAs were used in series instead of a single DB-PMA to ensure that the distal end of the soft arm moved horizontally by applying a different pressure at each SBCA. The modification increased the complexity of the system. However, the efficiency and the resulting performance and forms of the continuum arm were improved. The displacement amount depends on the design and size of the actuators.

As future work, a modification can be applied to the presented arm to enable the horizontal movement on both sides by adding two DB-PMAs in parallel but in an opposite layout.

Author Contributions: A.A.-I. designed and performed the experiments; A.A.-I. and S.D. analysed the data; A.A.-I. wrote the paper; and S.N.-M. edited the paper.

Acknowledgments: The authors would like to thank the Ministry of Higher Education (Iraq), University of Basrah, Computer-Engineering Department for providing scholarship support to the first author of this paper.

Conflicts of Interest: The authors declare no conflict of interest.

References

1. Fong, T.; Nourbakhsh, I.; Dautenhahn, K. A survey of socially interactive robots. *Robot. Autom. Syst.* **2003**, *42*, 143–166. [[CrossRef](#)]
2. Furuta, T.; Tawara, T.; Okumura, Y.; Shimizu, M.; Tomiyama, K. Design and construction of a series of compact humanoid robots and development of biped walk control strategies. *Robot. Autom. Syst.* **2001**, *37*, 81–100. [[CrossRef](#)]
3. Gouaillier, D.; Hugel, V.; Blazevic, P.; Kilner, C.; Monceaux, J.; Lafourcade, P.; Maisonnier, B. Mechatronic design of NAO humanoid. In Proceedings of the IEEE International Conference on Robotics and Automation, ICRA'09, Kobe, Japan, 12–17 May 2009.
4. Kaneko, K.; Kanehiro, F.; Kajita, S.; Yokoyama, K.; Akachi, K.; Kawasaki, T.; Isozumi, T. Design of prototype humanoid robotics platform for HRP. In Proceedings of the IEEE/RSJ International Conference on Intelligent Robots and Systems, Lausanne, Switzerland, 30 September–4 October 2002.
5. Leite, I.; Martinho, C.; Paiva, A. Social robots for long-term interaction: A survey. *Int. J. Soc. Rob.* **2013**, *5*, 291–308. [[CrossRef](#)]
6. Park, I.-W.; Kim, J.-Y.; Lee, J.; Oh, J.-H. Mechanical design of humanoid robot platform KHR-3 (KAIST humanoid robot 3: HUBO). In Proceedings of the 2005 5th IEEE-RAS International Conference on Humanoid Robots, Tsukuba, Japan, 5 December 2005.
7. Chou, C.-P.; Hannaford, B. Measurement and modeling of McKibben pneumatic artificial muscles. *IEEE Trans. Robot. Autom.* **1996**, *12*, 90–102. [[CrossRef](#)]
8. Tondou, B.; Lopez, P. Modeling and control of McKibben artificial muscle robot actuators. *IEEE Control Syst.* **2000**, *20*, 15–38. [[CrossRef](#)]
9. Davis, S.; Tsagarakis, N.; Canderle, J.; Caldwell, D.G. Enhanced modelling and performance in braided pneumatic muscle actuators. *Int. J. Rob. Res.* **2003**, *22*, 213–227. [[CrossRef](#)]
10. Szepe, T. Accurate force function approximation for pneumatic artificial muscles. In Proceedings of the 2011 3rd IEEE International Symposium on Logistics and Industrial Informatics (LINDI), Budapest, Hungary, 25–27 August 2011.
11. Ranjan, R.; Upadhyay, P.; Kumar, A.; Dhyani, P. Theoretical and Experimental Modeling of Air Muscle. *Int. J. Emerg. Technol. Adv. Eng.* **2012**, *2*, 112–119.
12. Al-Ibadi, A.; Nefti-Meziani, S.; Davis, S. Valuable experimental model of contraction pneumatic muscle actuator. In Proceedings of the 2016 21st International Conference on Methods and Models in Automation and Robotics (MMAR), Miedzyzdroje, Poland, 29 August–1 September 2016.
13. Al-Ibadi, A.; Nefti-Meziani, S.; Davis, S. Efficient structure-based models for the McKibben contraction pneumatic muscle actuator: The full description of the behaviour of the contraction PMA. *Actuators* **2017**, *6*, 32. [[CrossRef](#)]
14. Doumit, M.; Fahim, A.; Munro, M. Analytical modeling and experimental validation of the braided pneumatic muscle. *IEEE Trans. Robot.* **2009**, *25*, 1282–1291. [[CrossRef](#)]
15. Kelasidi, E.; Andrikopoulos, G.; Nikolakopoulos, G.; Manesis, S. A survey on pneumatic muscle actuators modeling. In Proceedings of the 2011 IEEE International Symposium on Industrial Electronics (ISIE), Gdansk, Poland, 27–30 June 2011.
16. Al-Ibadi, A.; Nefti-Meziani, S.; Davis, S. Novel models for the extension pneumatic muscle actuator performances. In Proceedings of the 2017 23rd International Conference on Automation and Computing (ICAC), Huddersfield, UK, 7–8 September 2017.
17. Ilievski, F.; Mazzeo, A.D.; Shepherd, R.F.; Chen, X.; Whitesides, G.M. Soft robotics for chemists. *Angew. Chem.* **2011**, *123*, 1930–1935. [[CrossRef](#)]
18. Deimel, R.; Brock, O. A compliant hand based on a novel pneumatic actuator. In Proceedings of the 2013 IEEE International Conference on Robotics and Automation (ICRA), Karlsruhe, Germany, 6–10 May 2013.
19. Al-Ibadi, A.; Nefti-Meziani, S.; Davis, S. Cooperative project by self-bending continuum arms. In Proceedings of the 2017 23rd International Conference on Automation and Computing (ICAC), Huddersfield, UK, 7–8 September 2017.

20. Al-Fahaam, H.; Davis, S.; Nefti-Meziani, S. The design and mathematical modelling of novel extensor bending pneumatic artificial muscles (EBPAMs) for soft exoskeletons. *Robot. Autom. Syst.* **2018**, *99*, 63–74. [[CrossRef](#)]
21. Faudzi, A.A.M.; Razif, M.R.M.; Nordin, I.N.A.M.; Suzumori, K.; Wakimoto, S.; Hirooka, D. Development of bending soft actuator with different braided angles. In Proceedings of the 2012 IEEE/ASME International Conference on Advanced Intelligent Mechatronics (AIM), Kachsiung, Taiwan, 11–14 July 2012.
22. Erkmen, I.; Erkmen, A.M.; Matsuno, F.; Chatterjee, R.; Kamegawa, T. Snake robots to the rescue! *IEEE Robot. Autom. Mag.* **2002**, *9*, 17–25. [[CrossRef](#)]
23. Transth, A.A.; Pettersen, K.Y.; Liljebäck, P. A survey on snake robot modeling and locomotion. *Robotica* **2009**, *27*, 999–1015. [[CrossRef](#)]
24. Hopkins, J.K.; Spranklin, B.W.; Gupta, S.K. A survey of snake-inspired robot designs. *Bioinspir. Biomim.* **2009**, *4*, 021001. [[CrossRef](#)] [[PubMed](#)]
25. Shan, Y.; Koren, Y. Design and motion planning of a mechanical snake. *IEEE Trans. Syst. Man Cybern.* **1993**, *23*, 1091–1100. [[CrossRef](#)]
26. Yamakita, M.; Yamada, T.; Tanaka, K. Control of snake like robot for locomotion and manipulation. In Proceedings of the 2nd International Symposium on Adaptive Motion of Animals and Machines, WeP-III, Kyoto, Japan, 4–8 March 2003.
27. Wright, C.; Buchan, A.; Brown, B.; Geist, J.; Schwerin, M.; Rollinson, D.; Choset, H. Design and architecture of the unified modular snake robot. In Proceedings of the 2012 IEEE International Conference on Robotics and Automation (ICRA), Saint Paul, MN, USA, 14–18 May 2012.
28. Wright, C.; Johnson, A.; Peck, A.; McCord, Z.; Naaktgeboren, A.; Gianfortoni, P.; Choset, H. Design of a modular snake robot. In Proceedings of the IEEE/RSJ International Conference on Intelligent Robots and Systems, IROS 2007, San Diego, CA, USA, 29 October–2 November 2007.
29. Hirose, S.; Yamada, H. Snake-like robots [tutorial]. *IEEE Robot. Autom. Mag.* **2009**, *16*, 88–98. [[CrossRef](#)]



© 2018 by the authors. Licensee MDPI, Basel, Switzerland. This article is an open access article distributed under the terms and conditions of the Creative Commons Attribution (CC BY) license (<http://creativecommons.org/licenses/by/4.0/>).